ACS OMEGA

http://pubs.acs.org/journal/acsodf

Article

Solution Phase Growth and Ion Exchange in Microassemblies of Lead Chalcogenide Nanoparticles

Swapnil D. Deshmukh, Kyle G. Weideman, Caleb K. Miskin, Kim Kisslinger, and Rakesh Agrawal*

Cite This: *ACS Omega* 2021, 6, 21350−21358

Read Online

ACCESS | Metrics & More | Article Recommendations | Supporting Information

ABSTRACT: We demonstrate the synthesis of micron-sized assemblies of lead chalcogenide nanoparticles with controlled morphology, crystallinity, and composition through a facile room-temperature solution phase reaction. The amine−thiol solvent system enables this synthesis with a unique oriented attachment growth mechanism of nanoparticles occurring on the time scale of the reaction itself, forming single-crystalline microcubes of PbS, PbSe, and PbTe materials. Increasing the rate of reaction by changing reaction parameters further allows disturbing the oriented attachment mechanism, which results in polycrystalline micro-assemblies with uniform spherical morphologies. Along with polycrystallinity, due to the differences in reactivities of each chalcogen in the solution, a different extent of hollow-core nature is observed in these microparticles. Similar to morphologies, the composition of such microparticles can be altered through very simplistic room-temperature solution phase coprecipitation, as well as ion-exchange reactions. While coprecipitation reactions are successful in synthesizing core−shell microstructures of PbSe−PbTe materials, the use of solution phase ion-exchange reaction allows for the exchange of not only Te with Se but also Ag with Pb inside the core of the PbTe microparticles. Despite exchanging one Pb with two Ag cations, the hollow-core nature of particles aids in the retention of the original uniform microparticle morphology.

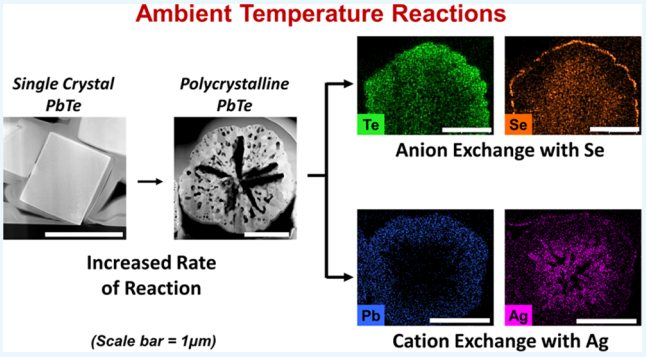

1. INTRODUCTION

The lead chalcogenide system is one of the most studied metal chalcogenide material systems in the past few decades. It has been used in two key electronic applications, one being quantum dot solar cells (QDSCs) and the other being thermoelectric (TE) devices. Lead chalcogenides like PbS and PbSe served as preliminary material systems, which allowed for a better understanding of quantum-scale electronic properties.[1,2] Although various efforts have been made to improve lead chalcogenide QDSC efficiencies, it has saturated at around 12%[3] and other QDSC material systems have recently surpassed this efficiency with the current record being 16.6% for colloidal perovskite quantum dot material.[4] However, in the field of TE devices, lead chalcogenides are still one of the highest performing material systems with ZT > 2.[5] Such high thermoelectric performance is generally measured for bulk, nanostructured lead chalcogenide materials produced in a complex and energy-intensive fashion. Fabrication of these high-performing devices is performed via high-temperature melt processing where an ingot of the desired composition is synthesized by melting metals together, followed by ball milling and hot pressing to get the desired material properties.[6] Beyond bulk systems, there are also various reports on the synthesis of lead chalcogenides in the form of nanoparticles, which allow for lower-intensity scalable printing options, as well as the incorporation of beneficial nano- and microstructuring in the device.[7] However, thin film devices fabricated with lead chalcogenide nanoparticles have issues like poor electrical conductivity due to multiple grain boundaries, incorporation of organic ligands, and difficulty in fabricating thicker films (>10 μm) when higher power generation density is required.[8,9] To resolve these issues, fabrication of thick-film TE devices by scalable printing has been demonstrated by utilizing ink/paste prepared using micron-sized particles.[8,10] However, these particles were still obtained by ball milling ingots of the desired material, suggesting poor control over particle uniformity and use of the energy-intensive ingot forming and ball milling processes. Development of a more facile and controlled route of microparticle synthesis via solution processing could provide great promise for TE device fabrication.

Received: March 24, 2021
Accepted: July 30, 2021
Published: August 11, 2021

https://doi.org/10.1021/acsomega.1c01589
ACS Omega 2021, 6, 21350−21358

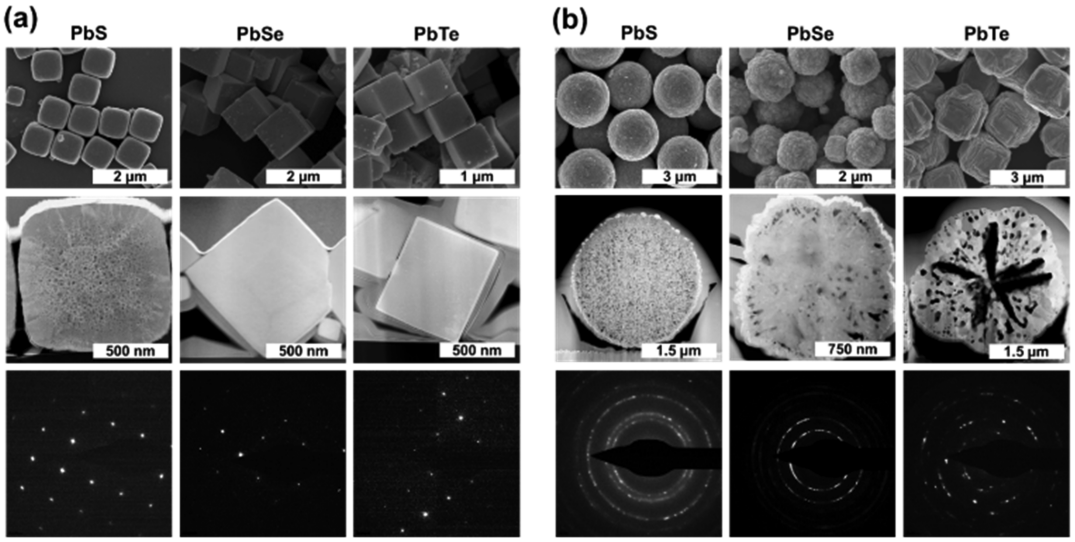

Figure 1. SEM, scanning transmission electron microscopy (STEM), and selected area electron diffraction (SAED) images for PbS, PbSe, and PbTe particles synthesized with (a) 5 mM reaction and (b) 100 mM reaction.

Another important parameter that must be attained for achieving high-performance TE devices is the ability to create compositional variation. Reports on lead chalcogenide TE devices show that PbSe incorporation in PbTe or vice versa is beneficial for improved performance. Similar to the chalcogen incorporation, composites of PbTe with Ag_2Te, Bi_2Te_3, SrTe, and many other materials have also proved to be viable routes for realizing ZT over 2.[11,12] Achieving such alloying, doping, or composite formation via solution phase chemistry is therefore as important as controlling microstructure uniformity. There are multiple reports in the literature for synthesizing nanoparticles with varied compositions in the form of either homogeneous alloys or heterogeneous structures (e.g., core−shell).[13−15] Along with direct synthesis, processes like ion exchange have proven to be quite successful in introducing composition variation in nanoparticles via solution routes.[16,17] While some work has been done in ion exchange of lead chalcogenide material, most of it is on nanoparticles and specifically on cation exchanges. Therefore, to achieve composition variation, it is necessary to develop a route suitable for incorporating foreign anions and cations in Pb chalcogenide microstructures either during or after the synthesis of the particles.

In this work, we achieved such microstructural morphologies with varied compositions for lead chalcogenide materials via a facile chemical route. Building upon our previous work where we demonstrated the room-temperature synthesis of lead chalcogenide materials in the form of nano- and microparticles,[18] here we investigated morphology control of the microstructures formed via this route. Techniques including transmission electron microscopy, selected area electron diffraction, and scanning transmission electron microscopy coupled with energy-dispersive X-ray spectroscopy were used to study the interior of these microstructures. Based on our results, we tuned the morphology of these microstructures by simply altering the synthesis conditions and achieved transition from single-crystal to polycrystalline microstructures. Interestingly, the results showed a hollow-core morphology for the PbTe system at high reactant concentrations, which make it attractive for application in TE devices. The composition of the microstructures was then tuned by utilizing the approaches of coprecipitation and ion-exchange reactions, which took advantage of the versatile solubility provided by amine−thiol solutions.[19] We successfully showed incorporation of Se in the PbTe structure via anion exchange at room temperature and used heat treatments to control its incorporation to get either core−shell composition or uniform alloying within the microstructure. Similarly, we studied exchanges with different cations, where we realized the successful exchange of Pb with Ag with complete retention of the microstructure morphology. While studying these exchanges with lead chalcogenide systems, we realized the formation of phase-pure Ag_2Te and Bi_2Te_3 materials using amine−thiol solutions, which are also well-known promising thermoelectric systems. As these reactions and ion exchanges were performed at room temperature via solution chemistry, they provide promise in terms of scalability and offer a route toward low-energy-intensity TE device fabrication.

2. RESULTS AND DISCUSSION

2.1. Microstructure Growth. Lead chalcogenide particle synthesis was performed using lead iodide and chalcogen solutions prepared with the amine−thiol solvent system. As reported previously, this synthesis route produces phase-pure lead chalcogenide materials in the form of microstructures when short-chain amines and thiols are used for the reaction.[18] To analyze these microstructures in detail and to study their growth process, different concentration reactions (5 and 100 mM) were performed for all three PbS, PbSe, and PbTe material systems. As described in the Experimental Section, ethylenediamine−ethanethiol (EN−ET) solvent mixture was used for PbSe and PbTe syntheses while the butylamine−ethanethiol (BA−ET) solvent mixture was used for PbS synthesis as no precipitation was observed for PbS particles when EN−ET was used for the reaction.[18]

Reactions performed at a 5 mM concentration showed precipitation of particles at around 1, 4, and 6 min after mixing for PbS, PbSe, and PbTe systems, respectively. These reaction mixtures were stirred for around 20 min to ensure complete conversion of the reactants. Particles recovered from these reactions, after washing as described in the Experimental Section, were analyzed for phase, composition, and morphol-

https://doi.org/10.1021/acsomega.1c01589
ACS Omega 2021, 6, 21350−21358

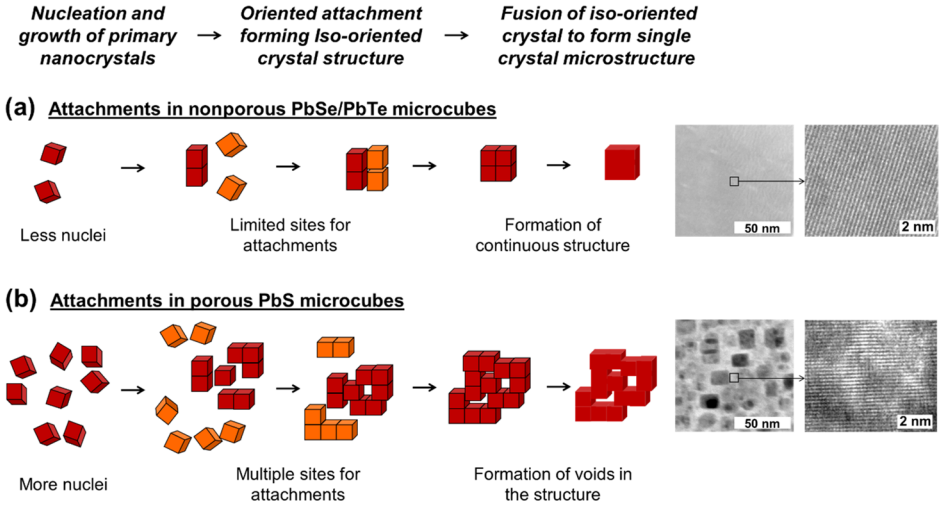

Figure 2. Proposed growth mechanism for the formation of single-crystal microstructures via oriented attachment and fusion in a 5 mM reaction scenario. (a) Top schematic represents the mechanism for relatively slower reaction (PbSe and PbTe), while (b) the bottom schematic represents the mechanism for relatively faster reaction (PbS).

ogy using X-ray diffractogram (XRD), X-ray fluorescence (XRF), and scanning electron microscopy (SEM), respectively. The XRF analysis performed on particles confirms the presence of lead and respective chalcogens, while the XRD pattern confirms the formation of phase-pure crystalline lead chalcogenide materials (Figure S1). SEM analysis of these particles shows the formation of cubical microstructures for all three lead chalcogenide systems with some morphological variations among them (Figure 1a). PbS cubes have rounded edges and corners, while cubes of PbSe and PbTe have sharp edges and corners. On average, the PbS and PbSe cubes are around 1 μm in size, while PbTe cubes are only around 500 nm despite similar reaction conditions. The PbS microstructures also appear relatively uniform in size and are isolated from each other when compared to the PbSe and PbTe particles, which show particle sizes with a couple of hundred nanometers of variations and some extent of physical contact between few submicron particles.

To gain more insight into these differences, lamellae were created from these microstructures for each system using focused ion beam (FIB) milling and then analyzed using transmission electron microscopy (TEM)/STEM. As can be seen in Figure 1a, PbSe and PbTe particles showed continuous cross section, while PbS particles showed a porous interior. When selected area electron diffraction (SAED) was performed to identify the crystallinity of these particles, surprisingly all microstructures were detected to be single crystals. While the formation of such single-crystal microstructures can be attained via homogeneous nucleation followed by the classical atom-by-atom growth, the presence of voids in PbS microstructures makes it seem less plausible.[20] On the other hand, there have been reports on the oriented attachment of nanoparticles in the literature where smaller nanoparticles orient themselves and attach to other nanoparticles such that it forms a three-dimensional (3D)/two-dimensional (2D) structure. With time, these 3D/2D structures have shown to transition from polycrystalline iso-oriented material to monocrystalline material through a process of fusion.[21,22] Although such an oriented assembly of nanoparticles has been studied in the literature to some extent, it is generally demonstrated after the synthesis of primary nanoparticles. However, if such an attachment mechanism indeed exists for this reaction, it would occur during the nanoparticle synthesis reaction, which makes it a unique phenomenon. So, to identify if these microstructures are indeed formed via agglomeration of nanoparticles, particles formed at the intermediate reaction time were analyzed by high-resolution SEM. As the reactions are relatively fast and quenching these reactions with any foreign solvent addition is not possible due to precipitation of unreacted reactants along with the particles, the reaction mixture itself was spin-coated during the course of reaction on a glass substrate and immediately washed with amine−thiol solvent. When these glass substrates were analyzed under SEM, a few particles with cubical morphology but smaller sizes (~200 to 300 nm) were observed. Interestingly, these intermediate cubical particles showed more textured faces along with the presence of nanoparticles on the surface when compared with fully grown particles, which supports the possibility for coalescence growth mechanism (Figure S2). Based on this result, we believe that smaller particles form in the solution near primary nuclei and then orient and arrange themselves to form an assembly, which fuses to result in a single-crystalline material (Figure 2a).

In this process, if nanoparticles do not get enough time to complete the orientation and rearrangement process, it could result in a noncontinuous structure. As the reaction for PbS synthesis is faster than PbSe/PbTe, at the start of the crystallization process, it could form a relatively higher number of nuclei in a short time and hence a higher concentration of nanoparticles. Such a high concentration of nanoparticles could provide multiple attachment sites and if the time scale for oriented attachment and nucleation of nanoparticles is comparable, formation of voids in the PbS structure can be realized, as illustrated in Figure 2b. Formation of voids during oriented attachment has been previously observed for microstructures of materials like $CaCO_3$ and ZnS, which suggests the likelihood of similar growth behavior in the PbS microstructures.[23,24] The presence of such voids only in the interior but not as much in the shell of the PbS microstructure further supports this mechanism as with increasing time, the concentration of reactant decreases in the solution, which

https://doi.org/10.1021/acsomega.1c01589
ACS Omega 2021, 6, 21350−21358

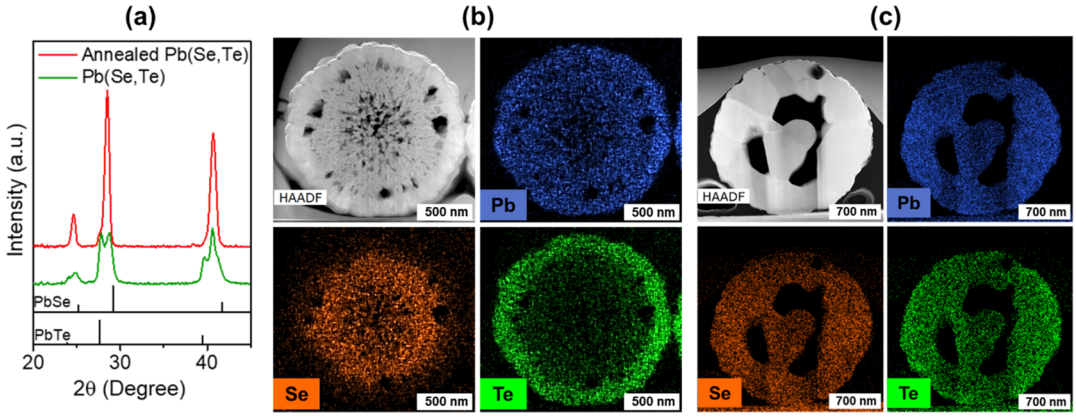

Figure 3. (a) XRD pattern of as-synthesized Pb(Se,Te) particles and 400 °C annealed Pb(Se,Te) particles showing transition from heterogeneous phase to homogeneous alloy (PbSe Std: ICSD 38294, PbTe Std: ICSD 38295). HAADF and STEM-EDS mapping of (b) as-synthesized and (c) 400 °C annealed Pb(Se,Te) particle.

results in a slower rate of reaction giving more time for orientation.

With this proposed understanding of the growth process in low-concentration reactions, the effect of a higher rate of reaction for all three systems on the microstructure morphology was studied by altering the reactant concentrations. When the reaction concentrations were increased by a factor of 20 (from 5 to 100 mM), the precipitation of particles in all three systems was observed instantaneously. This suggests a significantly higher rate of nucleation and reaction at these conditions. When analyzed in SEM, these particles showed spherical microstructures as expected based on our previous report. To study the interior of the microstructure, these spherical particles were also milled using FIB to make lamellae for TEM/STEM analysis. Unlike cubical particles, the cross sections of these spherical particles were significantly different for each material system. However, all of the structures were confirmed to be polycrystalline when analyzed with SAED (Figure 1b). In the case of PbS, STEM images showed uniform porosity in the interior of the microstructure without any specific shape of the pores, suggesting agglomeration of somewhat spherical nanoparticles. As the rate of reaction for this synthesis was high, the extent of homogeneous nucleation must be high as well, resulting in little to no time for oriented attachment. Hence, this would result in the formation of a polycrystalline agglomerated assembly. In the case of PbSe and PbTe, although the microstructures appeared polycrystalline, the TEM and STEM images revealed that the crystalline domains in these microstructures were relatively larger in size compared to those in PbS microstructures, which could be associated with their relatively slower rate of reactions. Unlike cubical structures, the spherical structures of PbSe and PbTe systems were quite different from each other. While both structures showed voids in the interior, the PbTe structure was significantly hollow in the core. To confirm the consistency of such an interesting hollow core, two more PbTe particles with slightly different sizes were analyzed under TEM/STEM, which also showed a similar extent of hollow core (Figure S3).

Although the reason for such a hollow core is not completely clear, one could hypothesize that, due to relatively slower reaction/nucleation, some extent of fusion could be taking place in the agglomerated structures. Assuming that original agglomeration has uniform porosity, with time, the particles that show more extent of fusion will lead to more and bigger voids in the core of the microstructures. As the rate of reaction follows the trend PbS > PbSe > PbTe, the extent of particle fusion would be expected to follow the reverse order, giving more void for the PbTe material. Alternatively, based on the chemical analysis of Se and Te solutions in the amine−thiol solvent system, it is known that different-sized chalcogen cluster ions are formed in the solution.[25] So, with a higher rate of reaction, some of the chalcogen clusters (i.e., Se_x or Te_x, where $x > 1$) could get trapped in the core of the particles at the start of assembly formation, which would eventually diffuse out to react on the surface leaving behind a void in the core of the particle.

2.2. Composition Control. *2.2.1. Coprecipitation Reaction.* While microstructures of different sizes, shapes, and crystallinities were synthesized using amine−thiol chemistry for PbS, PbSe, and PbTe material systems, PbTe microstructures are of prime attraction among these due to possible uses in thermoelectric applications. The hollow-core and polycrystalline domains in these microstructures promise an opportunity for selectively lowering the thermal conductivity, which could be beneficial for improving thermoelectric performance. Along with morphological variations, to get high thermoelectric performance, alloying and doping with foreign elements are proved to be necessary. One of the most successful routes to improve the performance is achieved via PbSe alloying. As amine−thiol chemistry is able to synthesize micron-sized PbTe and PbSe particles individually, it is hypothesized that the incorporation of both chalcogens (Se and Te) in the reaction mixture could form the desired Pb(Se,Te) alloy material through coprecipitation reaction.

To demonstrate the synthesis of a Pb(Se,Te) alloy material, Se and Te were codissolved in the EN−ET solution and then used for reaction with the PbI_2−EN−ET solution. Particles obtained from this reaction looked similar to the PbSe spherical microstructures, and when analyzed through X-ray diffraction, two different phases were observed (Figure 3a). This confirmed the formation of materials with heterogeneous phases; however, the SEM- energy-dispersive spectroscopy (EDS) analysis performed on these particles showed the presence of both Se and Te in the same microstructure (Figure S4). To get a detailed and clear mapping of elements, STEM-EDS was performed on a cross section of the particle. As can be seen from Figure 3b, the elemental mapping suggested the

https://doi.org/10.1021/acsomega.1c01589
ACS Omega 2021, 6, 21350−21358

formation of a core−shell structure. The shell of the microstructure was made of PbTe material, while the core was made of mostly PbSe material. Along with composition variation, it was very clear from the STEM image that the PbTe shell consisted of very dense material, while the PbSe core was relatively porous. This formation of a core−shell structure can be explained on the basis of the reactivity of Se and Te in the solution. Although at a 100 mM concentration, the reactions appeared instantaneous, it was observed that Te reacts relatively slower compared to Se when individual reactions were performed at lower concentrations, as described in the previous section. When both Se and Te are present in the solution, PbSe could be nucleating and growing first with some incorporation of Te, forming a Se-rich core, and then, with the selenium already precipitated out of solution, PbTe could be nucleating on the surface of this core to form the shell of the particle. When these core−shell structures were annealed at 400 °C for 5 min, the overall composition of particles measured using XRF remained unchanged. However, the XRD pattern collected on these annealed particles showed the presence of more crystalline materials with lattice parameters intermediate to those observed in the XRD pattern of non-annealed particles, suggesting some homogeneous alloying (Figure 3a). Further characterization of these annealed particles performed using STEM-EDS analysis supports the conclusions from XRD data and show the conversion from core−shell to uniformly distributed elemental composition along with the presence of larger crystalline domains in the microstructure (Figure 3c).

2.2.2. Anion Exchange. Although the successful introduction of PbSe in PbTe microstructures was achieved via coprecipitation route, the SEM analysis of different particles suggested a nonuniform size distribution. Importantly, the composition of these different-sized particles was realized to be different as shown in Figure S5 with the Se/(Se + Te) atomic ratio ranging from 0.48 to 0.80 between some of the analyzed particles. This variation was also observed with slightly nonsymmetric XRD peaks in Figure 3a. Such differences in composition could be a result of competing reactions in the solution and overall mixing and kinetic limitations. As both the chalcogens are present simultaneously in the solution, the mixing of solution could affect the extent of chalcogen incorporation. Similarly, while both chalcogens are getting consumed at different rates, the solution is undergoing a constant change in individual concentration and the relative ratio of Se/Te leading to nonuniformities in the particle compositions. To avoid such nonuniformity in size and composition during Se incorporation, an alternate route involving the process of ion exchange from Te to Se without altering the microstructure could be beneficial. However, anion exchanges are not as common as cation exchanges. Anions are generally large and form a rigid structure through which small cations can easily move and be replaced with new cations. On the other hand, when the anion needs to be replaced from the crystal structure, diffusion of the anion from the cation cage is difficult and may result in the disintegration of the structure, making it a less favorable process in many routes.[16,17] While there are a few reports on lead chalcogenide anion exchanges,[26,27] there is no report specifically on PbTe-to-PbSe exchange in the current literature to the best of our knowledge.

However, the amine−thiol solvent system exhibits unique chemistry with multiple similarities and differences identified among various chalcogen−amine−thiol solutions and could be exploited for ion-exchange reactions.[25] To study the feasibility of anion exchange in PbTe microstructures using the amine−thiol solvent system, a room-temperature solution approach was adopted. PbTe particles synthesized from the standard reaction with a 100 mM concentration were washed only with the amine−thiol solution after complete precipitation and then briefly dispersed in EN. These particles were then transferred in a 0.4 M Se−EN−ET solution to start the exchange process and were allowed to stir in this solution for 7 days. Four samples were collected from this solution after 2, 6, 24 h, and 7 days to study the extent of anion exchange as a function of time. The bulk elemental analysis performed using XRF showed the presence of Se in all samples, with Se/(Se + Te) atomic ratios of 0.25, 0.35, 0.70, and 0.80 for 2, 6, 24 h, and 7 day samples, respectively. This increasing Se/(Se + Te) ratio was also confirmed by XRD analysis, which showed reduction in the PbTe peak intensity and an increase in the PbSe peak intensity (Figure 4a). However, the presence of two different

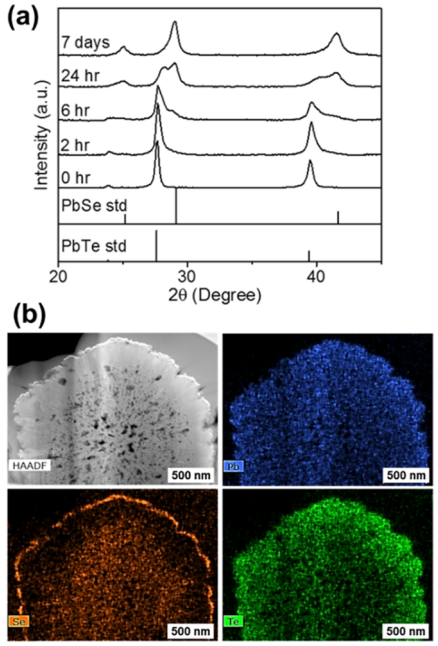

Figure 4. (a) XRD pattern of PbTe particles exchanged with the Se−EN−ET solution for different amounts of period (PbSe Std: ICSD 38294, PbTe Std: ICSD 38295). (b) HAADF and STEM-EDS elemental mapping of PbTe particle exchanged for 6 h with the Se−EN−ET solution.

XRD peaks in these samples suggested the formation of heterogeneous composite structures, which was further confirmed when the STEM-EDS analysis of a 6 h exchanged particle showed nonuniform elemental distribution within a single particle (Figure 4b). Like the precipitation method, these particles formed a core−shell structure with a Te-rich shell and a Se-rich core. This is a surprising result as one would expect a Se diffusion toward the center of the particle making PbSe shell and PbTe core. Such unexpected distribution can be realized if the microstructure shell allows Se solution to penetrate to the core through grain boundaries or porous surfaces. From Figure 1b, it can be seen that the starting PbTe particles have a dense shell and are porous in the core. If the Se liquid comes in contact with the core and the shell simultaneously, the relatively higher surface area available in

https://doi.org/10.1021/acsomega.1c01589
ACS Omega 2021, 6, 21350−21358

the core of the microstructure can lead to a higher incorporation of Se. This reasoning becomes even more prominent when the mapping data obtained through STEM-EDS analysis of another particle shown in Figure S6 shows higher Se incorporation in the region where the shell of the particle has some surface cavities. While the elemental distribution observed for the ion-exchanged particles was similar to that observed with the coprecipitation reaction, the SEM analysis showed a uniform size distribution for these particles (Figure S7). The Se and Te contents in ion-exchanged particles were also identical for different particles in one batch of exchange (e.g., all analyzed particles with 7 days of exchange showed a Se/(Se + Te) of 0.80), which proved the superiority of ion-exchange reaction over the direct precipitation method described earlier. Surprisingly, even after 7 days, with around 80% Se incorporation, the morphology of the microstructures remained intact (Figure S7), which promises the extension of this ion-exchange reaction beyond particles to applications such as thin films.

As PbSe is a thermodynamically stable compound compared to PbTe, the exchange from PbTe to PbSe is favored by lattice enthalpy.[17] However, the extent of ion exchange is driven not just by the lattice enthalpy of the starting and final material but also by the entropy of the exchange and the solvation/desolvation energies for the ions in the respective solvent.[16,17] Based on experiments, it is known that Se has a much higher solubility in an amine−thiol solution compared to Te, and Se can also help in solvation of the Te in these solutions.[25] Several such factors are important and could play a role while designing ion-exchange reactions. When the Te exchange of PbSe particles was studied, some extent of exchange was observed in these particles, even though the direction of this exchange is unfavorable with regard to lattice enthalpy. XRD and XRF data collected on these samples showed a relatively lower extent of anion exchange (Figure S8a), with only 45% of Te incorporation after 7 days of exchange. Similarly, when PbS particles were exposed to the Se−BA−ET solution for ion exchange, up to 55% of Se incorporation was observed in these particles (Figure S9a) within 7 days. These results emphasize the role of parameters other than lattice enthalpy (thermodynamic stability) on ion exchange.

2.2.3. Cation Exchange. With anion exchange of PbTe-to-Pb(Se,Te) microstructures being successful in the amine−thiol solution, a similar approach for cation exchange was utilized to introduce foreign cations in PbTe microstructures. A solution for Ag cation was prepared by dissolving AgCl in the EN−ET solvent mixture, which produced a homogeneous solution. Like anion exchange, PbTe particles were dispersed in the Ag ion solution and four samples were collected at different time intervals (2, 6, 24 h, and 7 days) to study the extent of ion exchange. Elemental analysis of these particles performed using XRF gave Ag/(Ag + Pb) atomic ratios of 0.27, 0.42, 0.78, and 0.96 for 2, 6, 24 h, and 7 day samples, respectively. Unlike anion exchange where PbTe and PbSe shared the same crystal structure, the XRD analysis of cation-exchanged particles showed a transition of cubic PbTe to monoclinic Ag_2Te (Figure 5a). Interestingly, all samples exposed to Ag solution showed a shift of PbTe XRD peaks to lower 2θ, suggesting an increase in the lattice constant of the PbTe crystal structure. Also, compared to original PbTe particles, the Ag_2Te formed via exchange exhibited lower crystallinity as can be seen from the reduced XRD signal. Surprisingly, even with different crystal structures and with differences in the oxidation states of

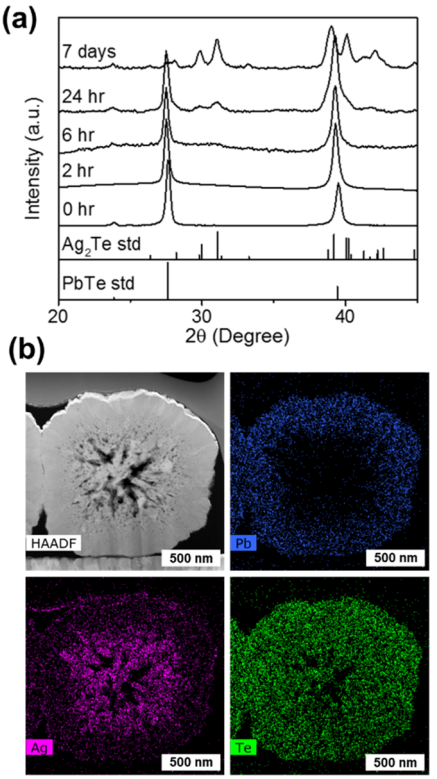

Figure 5. (a) XRD pattern of PbTe particles exchanged with the AgCl−EN−ET solution for different amounts of period (Ag_2Te Std: ICSD 73230, PbTe Std: ICSD 38295). (b) HAADF and STEM-EDS elemental mapping of PbTe particle exchanged for 24 h with the AgCl−EN−ET solution.

Ag and Pb, which leads to replacement of one Pb ion with two Ag ions (both ions having similar ionic radii, 129 pm for Ag^{+1} and 133 pm for Pb^{+2}), the microstructure of exchanged particles remained intact (Figure S10). This could be attributed to the void space within the microstructure, which may help in reducing the stress generated in cation exchange and provide the space for the crystal to grow and transform into a new crystal structure. To analyze the formation of Ag_2Te in the microstructure, STEM-EDS analysis was performed on the cross section of the 24 h exchanged particle (Figure 5b). The elemental mapping of this particle showed the formation of Ag_2Te only in the core of the particle, which is similar to the observation made with Se exchange particles and emphasizes the possible role of the void in retaining the morphology even after a drastic change in the number of cations. The retention of the morphology even with an almost complete conversion to Ag_2Te is also valuable as Ag_2Te itself is a promising low-temperature thermoelectric material[28] and such microstructures with a built-in polycrystallinity and porosity can be used for fabricating lead-free thermoelectric devices.

While cation like Ag showed successful exchange with Pb in PbTe particles, other cations like Na, Cd, Zn, and Bi did not show any exchange with Pb. The success of specific exchanges over others, like Ag → Pb over Cd → Pb even when CdTe is more stable and preferred over Ag_2Te, is surprising.[17] Similar to anion exchanges, these results suggest that the cation exchanges in the amine−thiol solvent system for PbTe materials could be driven by solvation and desolvation energies of the cations. To gain more insight into these differences, various metal salt solutions were prepared by dissolving AgCl,

https://doi.org/10.1021/acsomega.1c01589
ACS Omega 2021, 6, 21350−21358

NaSCN, $ZnCl_2$, $CdCl_2$, and $BiCl_3$ in the EN−ET solvent and then mixed with the Te solution prepared in the same solvent mixture. (The dissolution of $BiCl_3$ in the EN−ET solvent mixture resulted in precipitation of a small quantity of metallic Bi. This metallic Bi was filtered out from the solution and the rest of the solution (still containing Bi ions) was used for the reaction.) Most of these cation solutions remained homogeneous even after mixing with the Te solution, except for Ag and Bi, which formed a black color precipitate immediately after mixing. Similar precipitation was previously observed when Bi_2O_3 and Ag_2O solutions in amine−thiol were mixed with the Te solution in amine−thiol.[29] However, the XRF analysis of the precipitated particles in this study showed the presence of only Te and respective cation (Ag and Bi) with the absence of any other element, which was unique as the precipitate formed with Bi_2O_3 and Te solutions from the previous study showed incorporation of oxygen in the particles.[29] For AgCl-based reaction, the XRD analysis confirmed the formation of monoclinic Ag_2Te (Figure S11). However, the particles obtained with the $BiCl_3$ reaction did not show any XRD pattern, suggesting the formation of an amorphous material (Figure S12). When these particles were annealed at 300 °C for 5 min in an inert nitrogen atmosphere and then analyzed under XRD, the pattern confirmed transition from amorphous to crystalline trigonal Bi_2Te_3 material.

These results suggest that room-temperature ion exchanges in amine−thiol solutions are realized for material systems, which precipitate out as phase-pure chalcogenide materials at room temperature. As amine−thiol systems are also known to form materials like CdTe, ZnS, In_2S_3, and Cu_2Se when exposed to higher temperatures,[19,30] it is likely that anion and cation exchanges could be achieved with various other material systems if higher temperatures were to be utilized for the reactions.

3. CONCLUSIONS

We have demonstrated the synthesis of lead chalcogenide microstructures in different morphologies and compositions using facile room-temperature reactions in an amine−thiol solvent system. By altering the concentration of reactants in the solution, microstructures in the shape of cubes and spheres were synthesized for all three PbS, PbSe, and PbTe systems. Oriented attachment of particles was identified as a possible mechanism for growth of single-crystalline cubical microstructures. In contrast, spherical, polycrystalline morphologies synthesized via higher-concentration reactions showed a relatively hollow core. As hollow-core PbTe microstructures could have significant implication in thermoelectric devices, different composition variations for these structures were achieved via coprecipitation and ion-exchange reactions. Coprecipitation of Pb(Se,Te) material resulted in microstructures with the core−shell composition of PbSe and PbTe materials, which upon heat treatment were transformed to a uniform alloyed materials. However, the particles resulting from the coprecipitation method showed nonuniform particle size and composition among the particles. On the other hand, the process of room-temperature ion exchange was able to introduce foreign ions in PbTe microstructures with a uniform composition. With such ion-exchange process, successful incorporation of Se and Ag in PbTe particles resulted in core−shell structures with complete retention of the morphology. The extent of these ion exchanges was controlled with the duration of the exchange reactions. Although other cations like Na, Cd, Zn, and Bi did not result in ion exchange with Pb at room temperature, one could still exploit higher-temperature reactions with appropriate selection of amine−thiol pair for carrying out these exchanges and also extend its applicability to other metal chalcogenide systems.

4. EXPERIMENTAL SECTION

Materials. Lead(II) iodide (PbI_2, 99.999%), silver(I) chloride (AgCl, 99.999%), bismuth(III) chloride ($BiCl_3$, 99.998%), sodium(I) thiocyanate (NaSCN, 99.99%), zinc(II) chloride ($ZnCl_2$, 99.999%), cadmium(II) chloride ($CdCl_2$, 99.99%), sulfur powder (S, 99.98%), selenium powder (Se, 99.99%), tellurium powder (Te, 99.997%), n-butylamine (BA, 99.5%), ethanethiol (ET, >99%), and 1,2-ethylenediamine (EN, ≥99%) were purchased from Sigma-Aldrich and used without further purification.

Particle Synthesis. Lead chalcogenide particle synthesis was performed as described in our previous report. Lead iodide was dissolved in the amine−thiol (v/v = 1) solution at room temperature in one vial and a chalcogen (S/Se/Te) was dissolved in the same amine−thiol pair (v/v = 1) in another vial. After complete dissolution, both solutions were mixed together at room temperature to precipitate out lead chalcogenide particles. These particles were then washed once with the amine−thiol solution and then twice with isopropyl alcohol to remove any unreacted materials. For PbS synthesis, butylamine−ethanethiol solution was used, while for PbSe and PbTe synthesis, ethylenediamine−ethanethiol solution was used as solvent with an amine-to-thiol v/v ratio of 1. All solution preparations and reactions were performed in a nitrogen-filled glovebox, with oxygen and water contents maintained below 1 ppm. Spherical micron-sized particles of PbS, PbSe, and PbTe were obtained when reactions were performed using 100 mM lead iodide and chalcogen solutions. These reactions were instantaneous and completed within a few seconds. On the other hand, cubical micron-sized particles of PbS, PbSe, and PbTe were obtained when reactions were performed using 5 mM solutions of individual reactants. These reactions were slow and allowed to react for around 20 min for completion.

Ion-Exchange Procedure. Ion exchanges were performed at room temperature on various particles to study the incorporation of foreign cations and anions in the lead chalcogenide materials. For ion exchange, lead chalcogenide particles were first synthesized using the above-mentioned procedure. After synthesis, the particles were washed only once with the amine−thiol solution and then mixed with amine (BA for PbS and EN for PbSe and PbTe) without any exposure to isopropyl alcohol. Anion and cation solutions used for ion-exchange reactions were prepared in the amine−thiol solution (v/v = 1) using corresponding chalcogen and metal salt precursors. For anion exchange, 0.4 mmoles of PbTe particles (assuming a 100% yield during the particle formation process) in 100 μL of EN were transferred to 4 mL of a 0.4 M Se−EN−ET solution. Aliquots were collected at different time intervals to study the extent of Se incorporation in PbTe particles. Similarly, 0.4 mmoles of PbSe particles in 100 μL of EN and 0.4 mmoles of PbS particles in 100 μL of BA were transferred to 0.4 M chalcogen-based Te−EN−ET and Se−BA-ET solutions, respectively, to study the corresponding anion exchange as a function of time. For cation-exchange experiment, 0.4 mmoles of PbTe particles in 100 μL of EN were

https://doi.org/10.1021/acsomega.1c01589
ACS Omega 2021, 6, 21350−21358

transferred to 4 mL of a 0.4 M AgCl−EN−ET solution to study the incorporation of Ag in PbTe particles. Similar to anion exchange, aliquots were collected at different time intervals over a period of 1 week. All particles collected after aliquots were washed once with the corresponding amine−thiol solution followed by two isopropyl alcohol washes prior to any material characterization.

Characterization. X-ray diffractograms (XRDs) were obtained using a Rigaku Smart Lab diffractometer in the Bragg−Brentano mode using a Cu Kα (λ = 1.5406 Å) source operating at 40 kV/44mA. Scanning electron microscopy (SEM) images were collected using an FEI Quanta 3D SEM at an accelerating voltage of 10 kV, a spot size of 4.0, and a working distance of ∼10 mm using the Everhart Thornley Detector (ETD). The energy-dispersive spectroscopy (EDS) measurements were performed using an FEI Quanta 3D at 20 kV. EDS spectra were obtained using an Oxford INCA Xstream-2 silicon drift detector with an Xmax80 window and analyzed using Aztec software. Transmission electron microscopy (TEM) images and scanning transmission electron microscopy-EDS (STEM-EDS) data were collected on an FEI Talos 200X TEM. Samples for TEM analysis were prepared by cutting a cross section of particles using focused ion beam (FIB) in an FEI Helios SEM. Bulk nanoparticle composition was analyzed using a Fisher XAN 250 X-ray fluorescence (XRF) instrument.

■ ASSOCIATED CONTENT

Supporting Information

The Supporting Information is available free of charge at https://pubs.acs.org/doi/10.1021/acsomega.1c01589.

Additional SEM and TEM images for lead chalcogenide particles synthesized at various conditions and XRD of lead chalcogenide and ion-exchanged lead chalcogenide particles (PDF)

■ AUTHOR INFORMATION

Corresponding Author

Rakesh Agrawal − *Davidson School of Chemical Engineering, Purdue University, West Lafayette, Indiana 47907, United States;* orcid.org/0000-0002-6746-9829; Email: agrawalr@purdue.edu

Authors

Swapnil D. Deshmukh − *Davidson School of Chemical Engineering, Purdue University, West Lafayette, Indiana 47907, United States;* orcid.org/0000-0001-7101-7393

Kyle G. Weideman − *Davidson School of Chemical Engineering, Purdue University, West Lafayette, Indiana 47907, United States;* orcid.org/0000-0003-1541-3337

Caleb K. Miskin − *Davidson School of Chemical Engineering, Purdue University, West Lafayette, Indiana 47907, United States*

Kim Kisslinger − *Center for Functional Nanomaterials, Brookhaven National Laboratory, Upton, New York 11973, United States*

Complete contact information is available at: https://pubs.acs.org/10.1021/acsomega.1c01589

Notes

The authors declare no competing financial interest.

■ ACKNOWLEDGMENTS

The authors would like to acknowledge the funding support provided by the National Science Foundation under Grants 1534691-DMR (DMREF), 1735282-NRT (SFEWS), and 1855882 (INFEWS). The research was carried out, in part, at the Center for Functional Nanomaterials, Brookhaven National Laboratory, which is supported by the U.S. Department of Energy, Office of Basic Energy Sciences, under Contract No. DE-SC0012704.

■ REFERENCES

(1) Talapin, D. V.; Lee, J.-S.; Kovalenko, M. V.; Shevchenko, E. V. Prospects of Colloidal Nanocrystals for Electronic and Optoelectronic Applications. *Chem. Rev.* **2010**, *110*, 389−458.

(2) Moreels, I.; Lambert, K.; Smeets, D.; De Muynck, D.; Nollet, T.; Martins, J. C.; Vanhaecke, F.; Delerue, C.; Allan, G.; Hens, Z.; Vantomme, A. Size-Dependent Optical Properties of Colloidal PbS Quantum Dots. *ACS Nano* **2009**, *3*, 3023−3030.

(3) Baek, S. W.; Jun, S.; Kim, B.; Proppe, A. H.; Ouellette, O.; Voznyy, O.; Kim, C.; Kim, J.; Walters, G.; Song, J. H.; Jeong, S.; Byun, H. R.; Jeong, M. S.; Hoogland, S.; García de Arquer, F. P.; Kelley, S. O.; Lee, J. Y.; Sargent, E. H. Efficient Hybrid Colloidal Quantum Dot/Organic Solar Cells Mediated by near-Infrared Sensitizing Small Molecules. *Nat. Energy* **2019**, *4*, 969−976.

(4) Hao, M.; Bai, Y.; Zeiske, S.; Ren, L.; Liu, J.; Yuan, Y.; Zarrabi, N.; Cheng, N.; Ghasemi, M.; Chen, P.; Lyu, M.; He, D.; Yun, J. H.; Du, Y.; Wang, Y.; Ding, S.; Armin, A.; Meredith, P.; Liu, G.; Cheng, H. M.; Wang, L. Ligand-Assisted Cation-Exchange Engineering for High-Efficiency Colloidal Cs1−xFAxPbI3 Quantum Dot Solar Cells with Reduced Phase Segregation. *Nat. Energy* **2020**, *5*, 79−88.

(5) He, J.; Tritt, T. M. Advances in Thermoelectric Materials Research: Looking Back and Moving Forward. *Science* **2017**, *357*, No. eaak9997.

(6) He, R.; Schierning, G.; Nielsch, K. Thermoelectric Devices: A Review of Devices, Architectures, and Contact Optimization. *Adv. Mater. Technol.* **2018**, *3*, No. 1700256.

(7) Ortega, S.; Ibáñez, M.; Liu, Y.; Zhang, Y.; Kovalenko, M. V.; Cadavid, D.; Cabot, A. Bottom-up Engineering of Thermoelectric Nanomaterials and Devices from Solution-Processed Nanoparticle Building Blocks. *Chem. Soc. Rev.* **2017**, *46*, 3510−3528.

(8) Jo, S.; Choo, S.; Kim, F.; Heo, S. H.; Son, J. S. Ink Processing for Thermoelectric Materials and Power-Generating Devices. *Adv. Mater.* **2019**, *31*, No. 1804930.

(9) Ding, D.; Wang, D.; Zhao, M.; Lv, J.; Jiang, H.; Lu, C.; Tang, Z. Interface Engineering in Solution-Processed Nanocrystal Thin Films for Improved Thermoelectric Performance. *Adv. Mater.* **2017**, *29*, No. 1603444.

(10) Han, C.; Tan, G.; Varghese, T.; Kanatzidis, M. G.; Zhang, Y. High-Performance PbTe Thermoelectric Films by Scalable and Low-Cost Printing. *ACS Energy Lett.* **2018**, *3*, 818−822.

(11) Zhai, J.; Wang, T.; Wang, H.; Su, W.; Wang, X.; Chen, T.; Wang, C. Strategies for Optimizing the Thermoelectricity of PbTe Alloys. *Chin. Phys. B* **2018**, *27*, No. 047306.

(12) Su, C. H. Design, Growth and Characterization of PbTe-Based Thermoelectric Materials. *Prog. Cryst. Growth Charact. Mater.* **2019**, *65*, 47−94.

(13) Quan, Z.; Luo, Z.; Loc, W. S.; Zhang, J.; Wang, Y.; Yang, K.; Porter, N.; Lin, J.; Wang, H.; Fang, J. Synthesis of PbSeTe Single Ternary Alloy and Core/Shell Heterostructured Nanocubes. *J. Am. Chem. Soc.* **2011**, *133*, 17590−17593.

(14) Koktysh, D. S.; McBride, J. R.; Dixit, S. K.; Feldman, L. C.; Rosenthal, S. J. PbS/PbSe Structures with Core-Shell Type Morphology Synthesized from PbS Nanocrystals. *Nanotechnology* **2007**, *18*, No. 495607.

(15) Scheele, M.; Oeschler, N.; Veremchuk, I.; Peters, S. O.; Littig, A.; Kornowski, A.; Klinke, C.; Weller, H. Thermoelectric Properties of

Lead Chalcogenide Core-Shell Nanostructures. *ACS Nano* **2011**, *5*, 8541−8551.
(16) Li, X.; Ji, M.; Li, H.; Wang, H.; Xu, M.; Rong, H.; Wei, J.; Liu, J.; Liu, J.; Chen, W.; Zhu, C.; Wang, J.; Zhang, J. Cation/Anion Exchange Reactions toward the Syntheses of Upgraded Nanostructures: Principles and Applications. *Matter* **2020**, *2*, 554−586.
(17) De Trizio, L.; Manna, L. Forging Colloidal Nanostructures via Cation Exchange Reactions. *Chem. Rev.* **2016**, *116*, 10852−10887.
(18) Miskin, C. K.; Deshmukh, S. D.; Vasiraju, V.; Bock, K.; Mittal, G.; Dubois-Camacho, A.; Vaddiraju, S.; Agrawal, R. Lead Chalcogenide Nanoparticles and Their Size-Controlled Self-Assemblies for Thermoelectric and Photovoltaic Applications. *ACS Appl. Nano Mater.* **2019**, *2*, 1242−1252.
(19) McCarthy, C. L.; Brutchey, R. L. Solution Processing of Chalcogenide Materials Using Thiol−Amine "Alkahest" Solvent Systems. *Chem. Commun.* **2017**, *53*, 4888−4902.
(20) Thanh, N. T. K.; Maclean, N.; Mahiddine, S. Mechanisms of Nucleation and Growth of Nanoparticles in Solution. *Chem. Rev.* **2014**, *114*, 7610−7630.
(21) Nag, A.; Kundu, J.; Hazarika, A. Seeded-Growth, Nanocrystal-Fusion, Ion-Exchange and Inorganic-Ligand Mediated Formation of Semiconductor-Based Colloidal Heterostructured Nanocrystals. *CrystEngComm* **2014**, *16*, 9391−9407.
(22) Bahrig, L.; Hickey, S. G.; Eychmüller, A. Mesocrystalline Materials and the Involvement of Oriented Attachment-a Review. *CrystEngComm* **2014**, *16*, 9408−9424.
(23) Zhan, J.; Lin, H.-P.; Mou, C.-Y. Biomimetic Formation of Porous Single-Crystalline CaCO3 via Nanocrystal Aggregation. *Adv. Mater.* **2003**, *15*, 621−623.
(24) Yu, Y.; Chen, G.; Wang, Q.; Li, Y. Hierarchical Architectures of Porous ZnS-Based Microspheres by Assembly of Heterostructure Nanoflakes: Lateral Oriented Attachment Mechanism and Enhanced Photocatalytic Activity. *Energy Environ. Sci.* **2011**, *4*, 3652−3660.
(25) Deshmukh, S. D.; Easterling, L. F.; Manheim, J. M.; LiBretto, N. J.; Weideman, K. G.; Miller, J. T.; Kenttämaa, H. I.; Agrawal, R. Analyzing and Tuning the Chalcogen−Amine−Thiol Complexes for Tailoring of Chalcogenide Syntheses. *Inorg. Chem.* **2020**, *59*, 8240−8250.
(26) Ibáñez, M.; Hasler, R.; Liu, Y.; Dobrozhan, O.; Nazarenko, O.; Cadavid, D.; Cabot, A.; Kovalenko, M. V. Tuning P-Type Transport in Bottom-Up-Engineered Nanocrystalline Pb Chalcogenides Using Alkali Metal Chalcogenides as Capping Ligands. *Chem. Mater.* **2017**, *29*, 7093−7097.
(27) Hewavitharana, I. K.; Brock, S. L. When Ligand Exchange Leads to Ion Exchange: Nanocrystal Facets Dictate the Outcome. *ACS Nano* **2017**, *11*, 11217−11224.
(28) Chang, Y.; Guo, J.; Tang, Y. Q.; Zhang, Y. X.; Feng, J.; Ge, Z. H. Facile Synthesis of Ag2Te Nanowires and Thermoelectric Properties of Ag2Te Polycrystals Sintered by Spark Plasma Sintering. *CrystEngComm* **2019**, *21*, 1718−1727.
(29) McCarthy, C. L.; Webber, D. H.; Schueller, E. C.; Brutchey, R. L. Solution-Phase Conversion of Bulk Metal Oxides to Metal Chalcogenides Using a Simple Thiol-Amine Solvent Mixture. *Angew. Chem., Int. Ed.* **2015**, *54*, 8378−8381.
(30) Deshmukh, S. D.; Ellis, R. G.; Sutandar, D. S.; Rokke, D. J.; Agrawal, R. Versatile Colloidal Syntheses of Metal Chalcogenide Nanoparticles from Elemental Precursors Using Amine-Thiol Chemistry. *Chem. Mater.* **2019**, *31*, 9087−9097.

https://doi.org/10.1021/acsomega.1c01589
ACS Omega 2021, 6, 21350−21358